SCIENTIFIC REP⚙RTS

OPEN

Membrane Perturbation of ADP-insensitive Phosphoenzyme of Ca^{2+}-ATPase Modifies Gathering of Transmembrane Helix M2 with Cytoplasmic Domains and Luminal Gating

Stefania Danko, Kazuo Yamasaki, Takashi Daiho & Hiroshi Suzuki

Ca^{2+} transport by sarcoplasmic reticulum Ca^{2+}-ATPase involves ATP-dependent phosphorylation of a catalytic aspartic acid residue. The key process, luminal Ca^{2+} release occurs upon phosphoenzyme isomerization, abbreviated as E1PCa$_2$ (reactive to ADP regenerating ATP and with two occluded Ca^{2+} at transport sites) $\rightarrow$ E2P (insensitive to ADP and after Ca^{2+} release). The isomerization involves gathering of cytoplasmic actuator and phosphorylation domains with second transmembrane helix (M2), and is epitomized by protection of a Leu^{119}-proteinase K (prtK) cleavage site on M2. Ca^{2+} binding to the luminal transport sites of E2P, producing E2PCa$_2$ before Ca^{2+}-release exposes the prtK-site. Here we explore E2P structure to further elucidate luminal gating mechanism and effect of membrane perturbation. We find that ground state E2P becomes cleavable at Leu^{119} in a non-solubilizing concentration of detergent C$_{12}$E$_8$ at pH 7.4, indicating a shift towards a more E2PCa$_2$-like state. Cleavage is accelerated by Mg^{2+} binding to luminal transport sites and blocked by their protonation at pH 6.0. Results indicate that possible disruption of phospholipid-protein interactions strongly favors an E2P species with looser head domain interactions at M2 and responsive to specific ligand binding at the transport sites, likely an early flexible intermediate in the development towards ground state E2P.

Sarco(endo)plasmic reticulum (SR) Ca^{2+}-ATPase (expressed in adult fast-twitch skeletal muscle, SERCA1a), a representative member of P-type ion transporting ATPases, catalyzes Ca^{2+} transport coupled with ATP hydrolysis (Fig. 1) (for recent reviews, see Refs 1–3). The enzyme consists of three large cytoplasmic domains, Nucleotide binding (N), Phosphorylation (P), and Actuator (A), and ten transmembrane helices (M1~M10) (Figs 1 and 2). Ca^{2+} transport requires communication between the catalytic site on the cytoplasmic domains and the transport sites in the transmembrane helices *via* coupled structural changes, *i.e.* cytoplasmic domain motions and rearrangements of transmembrane helices. The enzyme is activated by the binding of two cytoplasmic Ca^{2+} ions at the high affinity transport sites composed of residues located on M4, M5, M6, and M8 (E2 to E1Ca$_2$ in Fig. 1). Then it is auto-phosphorylated at the catalytic residue Asp^{351} with ATP to form an ADP-sensitive phosphoenzyme (E1P), which is capable of reacting with ADP to regenerate ATP in the reverse reaction. Upon E1P formation, the two bound Ca^{2+} are occluded in the transport sites (E1PCa$_2$). The subsequent isomeric transition to the ADP-insensitive E2P form involves a large rotation of the A domain to associate with the P domain, thereby rearranging the Ca^{2+} binding sites to deocclude Ca^{2+}, open the release path (luminal gate), and reduce the affinity, thus allowing Ca^{2+} release into the lumen. As a consequence, the catalytic site in E2P is prepared for subsequent aspartyl phosphate hydrolysis by tightening of associated A and P domains. In the first step towards hydrolysis, progressing from the ground state to the transition state, namely E2P + H$_2$O $\rightarrow$ E2~P‡, the transport sites are protonated and the luminal gate closes tightly, preventing luminal Ca^{2+} access and driving the process forward[4,5].

Asahikawa Medical University, Department of Biochemistry, Midorigaoka-Higashi, Asahikawa, 078-8510, Japan. Correspondence and requests for materials should be addressed to H.S. (email: hisuzuki@asahikawa-med.ac.jp)
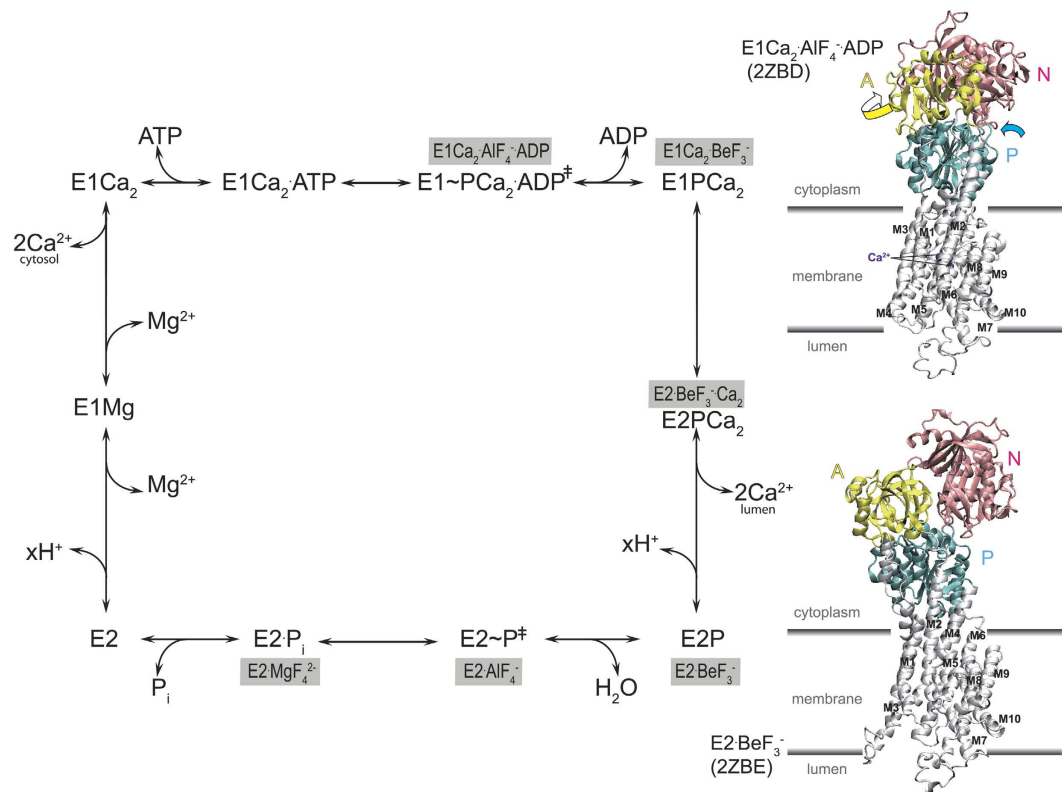
Figure 1. Reaction sequence of Ca^{2+}-ATPase. The sequence is shown with intermediates and transition states ($E1{\sim}PCa_2ADP^{\ddagger}$ and $E2{\sim}P^{\ddagger}$). Stable structural analog for each state developed with phosphate analogs BeF_3^{-}, AlF_4^{-} and MgF_4^{2-} [4,6,17,19] is shown with gray-highlight. In the crystal structures $E1Ca_2{\cdot}AlF_4^{-}{\cdot}ADP$ and $E2{\cdot}BeF_3^{-}$ (PDB code: 2ZBD[8] and 2ZBE[8], respectively), the cytoplasmic domains A (yellow), P (cyan), and N (pink), M1$\sim$M10, occluded two Ca^{2+}, and membrane position are indicated. Arrows on the domains in $E1Ca_2{\cdot}AlF_4^{-}{\cdot}ADP$ indicate their approximate motions to the $E2{\cdot}BeF_3^{-}$ structure to show changes in $E1PCa_2 \rightarrow E2P + 2Ca^{2+}$ as an available model.

The cytoplasmic part of the second transmembrane helix, M2, plays a crucial role in coupling A-domain motion and tilting of the P domain during the rearrangements of transport sites[4,6–9].

The $E2P$ ground state, transition state ($E2{\sim}P^{\ddagger}$), and product complex ($E2{\cdot}P_i$) in the $E2P$ hydrolysis process are mimicked by the stable structural analogs $E2{\cdot}BeF_3^{-}$, $E2{\cdot}AlF_4^{-}$, and $E2{\cdot}MgF_4^{2-}$, respectively, as produced with the respective phosphate analogs for different configurational states[4]. Their crystal structures, without or with the potent inhibitor thapsigargin (TG), have been solved at atomic level[7,8,10,11] following purification of the protein using a non-ionic detergent octaethylene glycol monododecyl ether ($C_{12}E_8$). Commensurate with the structural changes mentioned, the crystal structures are subtly different although the overall molecular structure of the compactly organized cytoplasmic A, P, and N domains with tightly bound BeF_3^{-} and occluded Mg^{2+} at the catalytic site and the arrangement of transmembrane helices are similar. Namely, the $E2{\cdot}BeF_3^{-}$ crystal produced at pH 7.0 in 50 mM Mg^{2+} has wide open transport sites (luminal gate open) with one bound Mg^{2+} [11] and that at pH 5.7, where the transport sites are protonated and Mg^{2+} is absent, the luminal access pathway is less open[8] (Fig. 2). The structures with bound TG at a cavity surrounded by M3, M5, and M7, namely $E2{\cdot}BeF_3^{-}$(TG), and those of $E2{\cdot}AlF_4^{-}$(TG) and $E2{\cdot}MgF_4^{2-}$(TG), are different again, and the luminal gate is tightly closed. The closure is associated with formation of hydrophobic interaction network, the Tyr^{122}-hydrophobic cluster (Y122-HC) by Leu^{119}/Tyr^{122} on the cytoplasmic part of M2 and five residues of the gathered A and P domains (Ile^{179}/Leu^{180} (A), Val^{705}/Val^{726} (P)) and A/M3-linker (Ile^{232} on the loop connecting the A domain with M3). Significantly, in the $E2{\cdot}BeF_3^{-}$ crystals without TG, where the gate is open, the side chains of Leu^{119}/Tyr^{122} are close but pointing away from the other gathered five residues, indicative of weaker domain interactions here (Fig. 2).

Extensive mutation and kinetic studies have demonstrated[12–15] that all seven residues involved in Y122-HC including Leu^{119}/Tyr^{122} are crucial for opening the gate, reducing Ca^{2+} affinity, and allowing rapid Ca^{2+}-release ($E2PCa_2 \rightarrow E2P + 2Ca^{2+}$), and for subsequent gate-closure and the formation of a catalytic site with hydrolytic ability. Investigation of the structural changes during these events has been aided by proteolytic digestion patterns, including a prtK site at Leu^{119} [4,16,17]. The site is exposed in the unphosphorylated $E2$ form but protected in $E2{\cdot}BeF_3^{-}$, $E2{\cdot}AlF_4^{-}$, and $E2{\cdot}MgF_4^{2-}$ as well as in the TG-bound forms of these analogs. Thus susceptibility to prtK attack or otherwise seems a good indicator of the state of the gathering of the head domains on M2. Significantly, $E2PCa_2$ an early $E2P$ species, is uniquely susceptible to attack, an indication of a loose arrangement of head domains on M2 prior to progression to ground state $E2P$ [4,18,19].
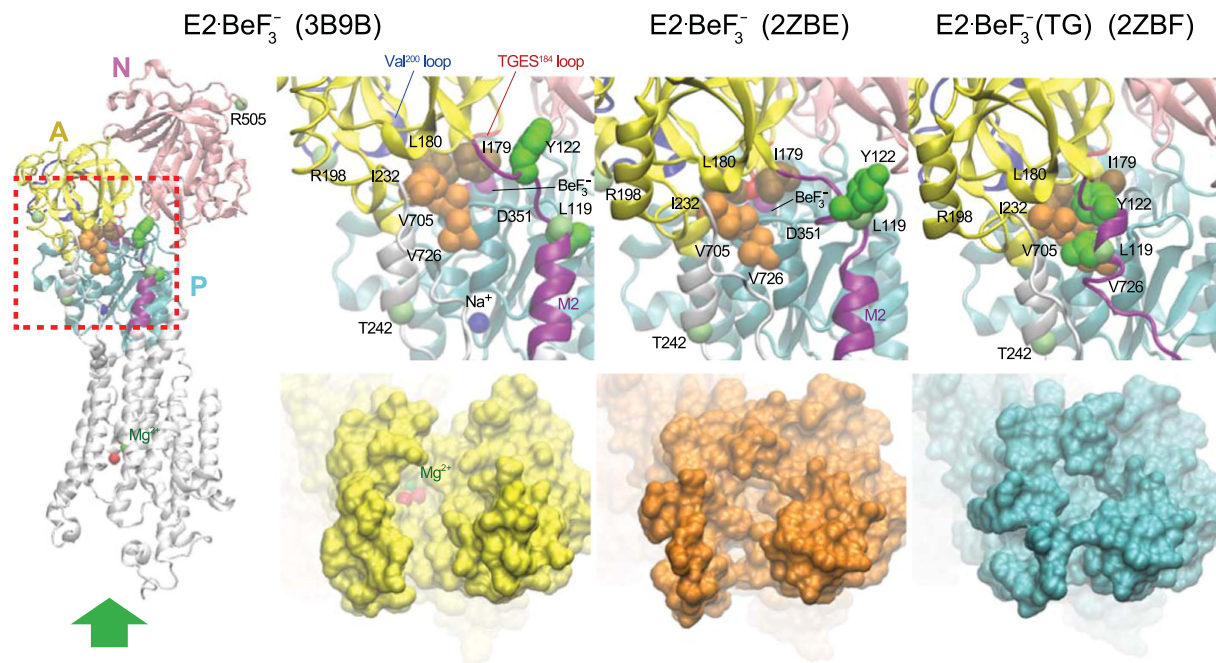
Figure 2. Crystal structures *E*2·BeF₃⁻ and *E*2·BeF₃⁻(TG). Structures *E*2·BeF₃⁻ with bound Mg²⁺ at the transport sites (formed at pH 7.0 and 50 mM Mg²⁺), *E*2·BeF₃⁻ with most probably protonated transport sites (formed at pH 5.7), and *E*2·BeF₃⁻(TG) (PDB code: 3B9B[11], 2ZBE[8], 2ZBF[8], respectively) are shown as a cartoon model. The cytoplasmic region indicated by the red broken line on the whole molecule of *E*2·BeF₃⁻ with bound Mg²⁺ is enlarged in the three top panels. In the three bottom panels, the view of transport sites from the luminal side as indicated by a large green arrow is shown. The A, P, and N domains and cytoplasmic part of M2 are yellow, cyan, pink, and purple, respectively. The Mg²⁺ and water molecules at the Ca²⁺ binding sites (transport sites) and Na⁺ bound at the K⁺ (Na⁺) site on the P domain are green, red, and blue spheres, respectively. The seven residues involved in the formation of Tyr¹²²-hydrophobic cluster, Y122-HC (Leu¹¹⁹/Tyr¹²² on M2, Ile¹⁷⁹/Leu¹⁸⁰ on the A domain, Val⁷⁰⁵/Val⁷²⁶ on the P domain, and Ile²³² on the A/M3-linker) are shown with van der Waals spheres, and colored green (Leu¹¹⁹/Tyr¹²²), brown (Ile¹⁷⁹/Leu¹⁸⁰), and orange (Val⁷⁰⁵/Val⁷²⁶/Ile²³²). The BeF₃⁻ coordinated in the catalytic site behind the residues involved in Y122-HC is shown by a space-filling model (cyan for beryllium and purple for fluoride) and Asp³⁵¹ (the auto-phosphorylation site) is shown in a ball-stick model in the panels (note that they are obscured by Y122-HC in *E*2·BeF₃⁻(TG)). The Mg²⁺ bound to the catalytic site is not depicted as it is also hidden by Y122-HC. The TGES¹⁸⁴ loop and Val²⁰⁰ loop (Lys¹⁸⁹-Lys²⁰⁵) are colored by a red loop and a blue loop, respectively in all panels. The prtK-cleavage sites at Leu¹¹⁹ and Thr²⁴² and the trypsin-cleavage sites at Arg¹⁹⁸ and Arg⁵⁰⁵ are indicated (backbone carbon).

Unexpectedly, we now find that low, non-solubilizing concentrations of $C_{12}E_8$ render the prtK site at Leu¹¹⁹ in *E*2P (*E*2·BeF₃⁻) susceptible to attack. It is as though the detergent has released constraints at the transmembrane helices to favor a state closer to that on Ca²⁺ binding to the luminal sites, namely *E*2PCa₂. The phenomenon uncovers a hitherto undescribed intermediate just prior to ground state *E*2P, stabilized by detergent that is uniquely susceptible to diverse ligand binding and cross-protein conformational changes. It shows that phospholipid-protein interactions directly participate the conformational changes associated with luminal gating events and expedite Ca²⁺ release.

Results

PrtK-cleavage of Leu¹¹⁹-site in *E*2·BeF₃⁻ with $C_{12}E_8$ at pH 7.4. In Fig. 3a, prtK-proteolysis of *E*2·BeF₃⁻ is performed at pH 7.4 in 0.1 M K⁺ without and with a non-solubilizing low concentration of $C_{12}E_8$. In the absence of $C_{12}E_8$, *E*2·BeF₃⁻ is completely resistant to prtK both without and with A23187 as found previously[4]. In the presence of $C_{12}E_8$, a 95-kDa fragment (p95) is produced by specific prtK-cleavage at the Leu¹¹⁹-site without any other cleavages. Cleavage is accelerated by 30 mM Mg²⁺, but no cleavage occurs in the absence of $C_{12}E_8$ even at 30 mM Mg²⁺. In Fig. 3d, the Mg²⁺ concentration dependence of the specific prtK-cleavage rate at the Leu¹¹⁹-site is determined in $C_{12}E_8$ and different monovalent cations (K⁺, Na⁺, and Li⁺) at 0.1 M. The rate increases with increasing Mg²⁺ concentration – binding to a low affinity site favors exposure. The cleavage is faster in Na⁺ and K⁺ as compared with that in Li⁺ or in the absence of monovalent cation, thus K⁺ or Na⁺ binding at the K⁺ site on the P domain[20,21] increases prtK attack at Leu¹¹⁹.

*E*2·BeF₃⁻ cleavage in $C_{12}E_8$ is inhibited by thapsigargin (TG), which binds tightly to a cavity surrounded by M3, M5, and M7, fixing the arrangement of transmembrane helices with a tightly closed luminal gate[22,23] (Fig. 3a "$C_{12}E_8$ + TG" for *E*2·BeF₃⁻). On the other hand, in the BeF₃⁻-free state with bound TG ("*E*2·TG") with Mg²⁺ as
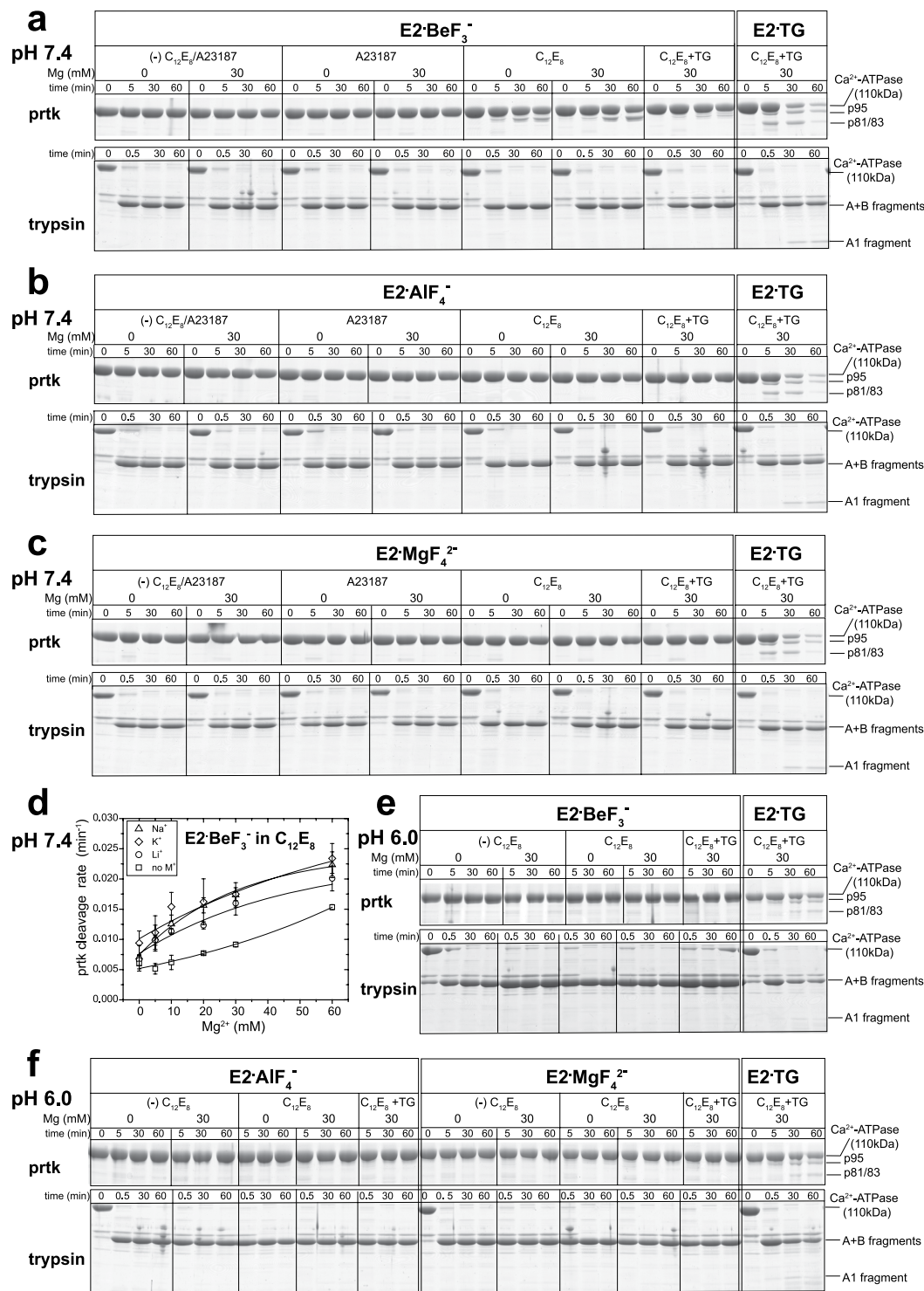
Figure 3. Effects of $C_{12}E_8$ and various factors on proteolysis of $E2 \cdot BeF_3{}^-$, $E2 \cdot AlF_4{}^-$, and $E2 \cdot MgF_4{}^{2-}$. The proteolysis was performed for various times with prtK and trypsin as indicated with $E2 \cdot BeF_3{}^-$ (**a,e**), $E2 \cdot AlF_4{}^-$ (**b,f**), and $E2 \cdot MgF_4{}^{2-}$ (**c,f**) of SR vesicles in the presence or absence of 0.15 mg/ml $C_{12}E_8$ or 15 μM A23187 in 50 mM MOPS/Tris pH 7.4 (**a–c**) or MES/Tris pH 6.0 (**e,f**), 0.1 M KCl, 1 mM EGTA, and 0 or 30 mM $MgCl_2$ without or with 4 μM TG ("TG"), as indicated. The "$E2 \cdot TG$" state of SR vesicles un-treated with the metal fluoride was subjected to the proteolysis as a control. In (**d**), the rate of prtK digestion of 110 kDa-ATPase chain in $C_{12}E_8$ at pH 7.4 was determined at various concentrations of $MgCl_2$ in 0.1 M KCl, NaCl, or LiCl or in the absence of these salts, otherwise as in (**a**) and as described under "METHODS". The fragments indicated on the right of a panel are p95 produced by the prtK-cleavage at the Leu[119]-site on M2, p81/p83 produced by the prtK-cleavage at the Thr[242]-site on A/M3-linker (p83) and Ala[746] on M5 (p81)[16,39], and the tryptic A1 fragment produced by cleavage at the Arg[198]-site on the A fragment (N-terminal half), which is formed very rapidly together with the B fragment (C-terminal half) by cleavage at Arg[505]-site[40].

well as without Mg^{2+}, the 110-kDa ATPase chain is very rapidly cleaved producing p95 and p81/p83 fragments by cleavages at Leu^{119} and at Thr^{242} (p83) and Ala^{746} (p81), respectively, in agreement with previous findings[16].

Tryptic T2 (Arg^{198})-site in $E2 \cdot BeF_3^-$ is completely resistant in $C_{12}E_8$.

The association of the Val^{200} loop (Lys^{189}-Lys^{205}) on the A domain with the P domain by ionic interactions is crucial for $E2P$ structure formation and occurs as a consequence of the A domain's large rotation during the $E1PCa_2 \rightarrow E2P$ isomeric transition[6,7,24]. With the changes, the Arg^{198}-tryptic T2 site in this loop becomes completely resistant to tryptic attack[4,6]. In Fig. 3a, the trypsin proteolysis was performed as described above with prtK. In the BeF_3^--free state with bound TG as a control ("$E2 \cdot TG$") in which the A and P domains are not fixed, the Arg^{198}-site is cleaved producing the A1 and A2 fragments (the A2 fragment is not seen because it is at the gel front) as found previously[6]. In $E2 \cdot BeF_3^-$, the A1 and A2 fragments are not produced regardless of the presence of $C_{12}E_8$ and 30 mM Mg^{2+}, thus the Arg^{198}-site is completely resistant, consistent with association of the A and P domains by an ionic network as seen in the $E2 \cdot BeF_3^-$ crystal structures[8,11].

$E2 \cdot BeF_3^-$ in $C_{12}E_8$ is completely resistant to prtK at pH 6.0.

In Fig. 3e, prtK-proteolysis was performed at pH 6.0 otherwise as in Fig. 3a. At this pH the luminal transport sites are expected to be protonated. No cleavage of the 110 kDa-ATPase chain occurred even in $C_{12}E_8$ and 30 mM Mg^{2+}. The tryptic Arg^{198}-site was also completely resistant at pH 6.0 as at pH 7.4 without and with $C_{12}E_8$ and 30 mM Mg^{2+}.

$E2 \cdot AlF_4^-$ and $E2 \cdot MgF_4^{2-}$ are completely resistant to prtK even in $C_{12}E_8$ at pH 7.4 and 6.0.

$E2 \cdot AlF_4^-$, the analog for the transition state $E2\sim P^{\ddagger}$ is completely resistant to prtK at pH 7.4 and 6.0 even in the presence of $C_{12}E_8$ both without and with 30 mM Mg^{2+} (Fig. 3b,f). The Arg^{198}-site is also protected from trypsin in all these conditions. $E2 \cdot MgF_4^{2-}$, the analog for the product complex ($E2 \cdot P_i$) is completely resistant to prtK and to trypsin in all these conditions as $E2 \cdot AlF_4^-$ (Fig. 3c,f).

Hydrophobic nature of the nucleotide/catalytic site revealed by TNP-AMP superfluorescence.

TNP-AMP binds to the ATP binding site with a very high affinity and develops an extremely high "superfluorescence" in the $E2P$ ground state and its analog $E2 \cdot BeF_3^{-}$[4,25]. The TNP moiety binds at the adenine position in the N domain and the superfluorescence can be ascribed to a favorable TNP moiety Phe^{487} interaction and site-occlusion that excludes non-specific water and increases hydrophobicity by the contribution of Arg^{174} on the A domain at the A-N interface on the TNP binding pocket[26]. The superfluorescence is completely lost during $E2P + H_2O \rightarrow E2\sim P^{\ddagger}$, as demonstrated with the change $E2 \cdot BeF_3^- \rightarrow E2 \cdot AlF_4^-$[4], probably through TNP-Phe^{487} mal-alignment and water influx here. In Fig. 4, the superfluorescence development in $E2 \cdot BeF_3^-$ upon the TNP-AMP binding at saturating $4\,\mu M$ was examined without and with $C_{12}E_8$ at pH 7.4 and 6.0 and various concentrations of Mg^{2+} in 0.1 M K^+ or Li^+. There was almost no effect of $C_{12}E_8$ on superfluorescence development. Specific K^+ binding on the P domain[20,21] also had virtually no effect (compare the data in K^+ with those in Li^+). Increasing Mg^{2+} concentration up to 60 mM caused only slight decrease. The results show that the catalytic/nucleotide site, starting from the $E2P$ ground state, is not affected by $C_{12}E_8$, Mg^{2+}, K^+, and protonation of transport sites.

$E2 \cdot BeF_3^-$ in $C_{12}E_8$ and Mg^{2+} is resistant to luminal Ca^{2+}-induced reverse conversion to $E1Ca_2 \cdot BeF_3^-$.

The $E2P$ ground state possesses luminally partially open low affinity transport sites and luminal Ca^{2+} at sub-mM to ~mM concentration is able to bind and cause reverse isomerization $E2P + 2Ca^{2+} \rightarrow E2PCa_2 \rightarrow E1PCa_2$, which contributes to the proper setting of luminal Ca^{2+} concentration through "back-door inhibition". This reverse process as well as the forward EP isomerization is mimicked and characterized with the structural analogs $E2 \cdot BeF_3^-$ ($E2P$), $E2 \cdot BeF_3^- \cdot Ca_2$ ($E2PCa_2$, the transient intermediate state before the Ca^{2+}-release), and $E1Ca_2 \cdot BeF_3^-$ ($E1PCa_2$)[4,17–19]. In Figs 5 and 6, the effect of luminal Ca^{2+} on $E2 \cdot BeF_3^-$ was examined at pH 7.4 in $C_{12}E_8$ or A23187, various concentrations of Mg^{2+}, and 0.1 M K^+ or Li^+. Here it should be noted that the $E1Ca_2 \cdot BeF_3^-$ complex is not stable and rapidly decomposes to $E1Ca_2$ in the presence of a high concentration of Ca^{2+} (due to Ca^{2+}-substitution at the unoccluded catalytic Mg^{2+} site in $E1Ca_2 \cdot BeF_3^{-}$[17]), on the other hand, it is very rapidly isomerized to $E2 \cdot BeF_3^-$ releasing Ca^{2+} upon the removal or reduction of luminal free Ca^{2+} concentration (to below ~100 μM) as the process mimics the isomeric transition $E1PCa_2 \rightarrow E2P + 2Ca^{2+}$[17]. Also, the $E1Ca_2 \cdot BeF_3^-$ complex decomposes to $E1Ca_2$ upon ADP binding, mimicking the ADP-induced reverse dephosphorylation of $E1PCa_2$, and upon TNP-AMP binding probably analogous to the ADP-induced process, in contrast to a stable $E2 \cdot BeF_3^-$ with bound ADP or TNP-AMP[17].

In Fig. 5, taking these known properties into account, we first determined the overall time course of the Ca^{2+}-induced $E2 \cdot BeF_3^-$ reverse conversion and decomposition to $E1Ca_2$ ($E2 \cdot BeF_3^- + 2Ca^{2+} \rightarrow E2 \cdot BeF_3^- \cdot Ca_2 \rightarrow E1Ca_2 \cdot BeF_3^- \rightarrow E1Ca_2$) by adding an excess EGTA after various times of incubation with 0.5 mM Ca^{2+} thereby converting the remaining $E1Ca_2 \cdot BeF_3^-$ to the stable $E2 \cdot BeF_3^-$ species, and in addition adding TNP-AMP to determine superfluorescence development to estimate the total amount of $E2 \cdot BeF_3^-$ and $E1Ca_2 \cdot BeF_3^-$ species remaining at the time of EGTA addition. In Fig. 6, prtK proteolysis was performed for a short period during the 0.5 mM Ca^{2+} incubation and without the EGTA addition to identify the structural states of EP species under representative conditions in Fig. 5 (although the Ca^{2+}-induced process proceeds).

First in Fig. 5 where TNP-AMP superfluorescence is examined, we found both with K^+ and without K^+ (with LiCl) that the Ca^{2+}-induced reverse conversion/decomposition of $E2 \cdot BeF_3^-$ is considerably slower in $C_{12}E_8$ than in A23187, and increasing Mg^{2+} to ~20 mM in $C_{12}E_8$ causes a marked retardation or almost complete inhibition. The retardation by Mg^{2+} in $C_{12}E_8$ is much stronger and occurs at much lower Mg^{2+} concentration than in A23187. In the absence of both $C_{12}E_8$ and A23187, i.e. with an impermeable SR membrane, no conversion nor decomposition of $E2 \cdot BeF_3^-$ occurs with Ca^{2+}, therefore the Ca^{2+}-induced decomposition is due to the Ca^{2+} access from
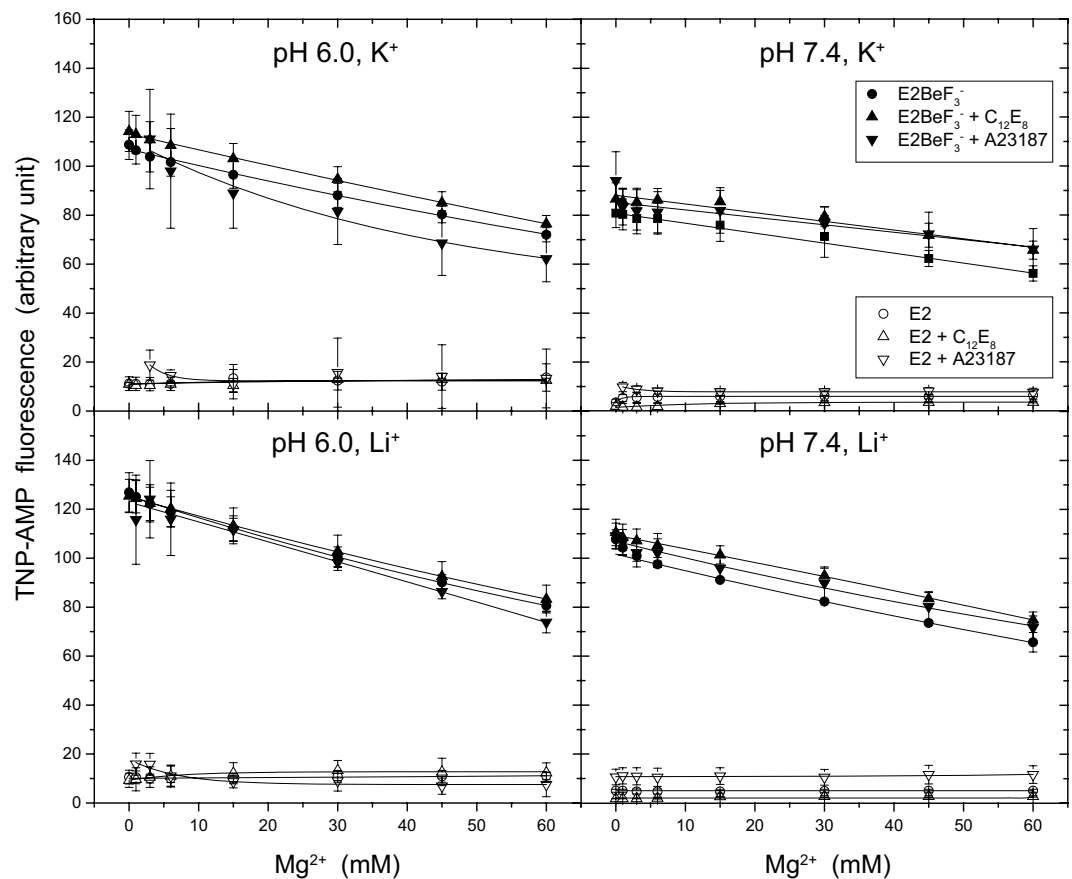
Figure 4. Hydrophobic property at nucleotide/catalytic site in $E2 \cdot BeF_3^-$ revealed by TNP-AMP superfluorescence. $E2 \cdot BeF_3^-$ or the BeF_3^--free Ca^{2+}-ATPase (*E2*) in SR vesicles (0.06 mg protein/ml) were incubated at 25 °C for 3 min in 0.5 mM EGTA, 30 mM MES/Tris (pH 6.0) or MOPS/Tris (pH 7.4), 0.1 M KCl or LiCl, and 0–60 mM $MgCl_2$ with or without 0.02 mg/ml $C_{12}E_8$ and/or 2.5 μM A23187, as indicated in the figure. Subsequently, TNP-AMP at saturating 4 μM was added. The fluorescence intensity was obtained by subtracting the protein background level without TNP-AMP and the level of 4 μM TNP-AMP without SR vesicles, and plotted *versus* Mg^{2+} concentration.

the luminal side as found previously[4,17]. Regarding the K^+ effect, the luminal Ca^{2+}-induced conversion/decomposition of $E2 \cdot BeF_3^-$ is considerably faster in K^+ than in its absence, therefore specific K^+ binding[20,21] accelerates the process.

Then in Fig. 6a, prtK-proteolysis was performed to identify the structural state stabilized in $C_{12}E_8$ with, most typically, 30 mM Mg^{2+} in the absence of K^+ during luminal Ca^{2+}-induced $E2 \cdot BeF_3^-$ reverse conversion and decomposition. Here, the sample was incubated first with 0.5 mM Ca^{2+} for 10 s, and then with a high concentration of prtK for various times without removal of Ca^{2+}. The proteolytic pattern was compared with those of BeF_3^--free $E1Ca_2$ and of $E1Ca_2 \cdot BeF_3^-$ that is formed and stabilized perfectly under the previously identified most appropriate conditions, *i.e.* at pH 7.0 with 0.7 mM Ca^{2+} and 15 mM Mg^{2+} in 0.1 M K^+ in the absence or presence of A23187 [17]; in these states, p81/p83 fragments are produced due to cleavage at Thr[242] (p83) and Ala[746] (p81) without production of the p95-fragment (Fig. 6b). In $C_{12}E_8$ and Ca^{2+} (Fig. 6a), $E2 \cdot BeF_3^-$ both without and with 30 mM Mg^{2+} is degraded slowly as compared with $E1Ca_2$, producing the stable p95 fragment as seen with $E2 \cdot BeF_3^-$ in $C_{12}E_8$ without Ca^{2+} (*cf.* Fig. 3) and a small amount of p81/p83 fragments, which degrade rapidly as the BeF_3^--free $E1Ca_2$ state. Note also that the 110-kDa ATPase chain degradation is much slower and formation of the rapidly degrading p81/p83 fragments is much less in 30 mM Mg^{2+} than without Mg^{2+}. The results show that $E2 \cdot BeF_3^-$ in $C_{12}E_8$ and Ca^{2+} is resistant to the luminal Ca^{2+}-induced reverse conversion to $E1Ca_2 \cdot BeF_3^-$, which can be interpreted as very slow Ca^{2+} binding to luminal transport sites and what slow conversion occurs is markedly retarded by 30 mM Mg^{2+}. These results accord with those using superfluorescence as the indicator in Fig. 5.

In the presence of A23187, as seen in Fig. 6a, formation of the p81/p83 fragments from $E2 \cdot BeF_3^-$ in Ca^{2+} occurs without any p95 fragment, as with $E1Ca_2$ and $E1Ca_2 \cdot BeF_3^-$ in A23187 (*cf.* Fig. 6b) indicating a fast conversion of $E2 \cdot BeF_3^-$ to $E1Ca_2 \cdot BeF_3^-$ without the detergent and with the ionophore. These results together with the retardation by Mg^{2+} of loss of TNP-AMP superfluorescence (Fig. 5) indicate that $E1Ca_2 \cdot BeF_3^-$ is formed from $E2 \cdot BeF_3^-$ without detergent on luminal Ca^{2+} binding and further decomposed to $E1Ca_2$, and that Mg^{2+} at a high
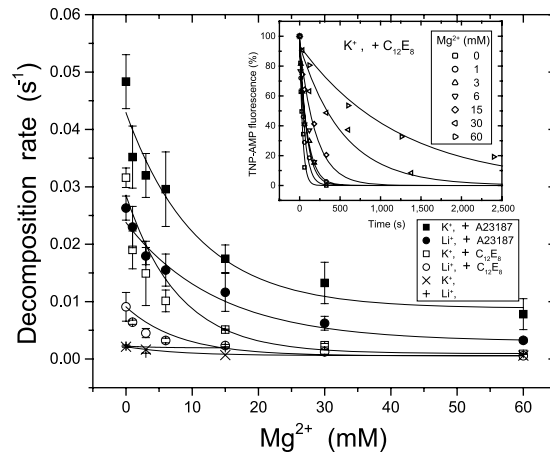
Figure 5. Luminal Ca²⁺-induced reverse conversion and decomposition of $E2 \cdot BeF_3^-$ determined by loss of TNP-AMP superfluorescence. $E2 \cdot BeF_3^-$ in SR vesicles was incubated at 25 °C for 3 min in 30 mM MOPS/Tris (pH 7.4), 0.1 M KCl or LiCl, 0.5 mM EGTA, 0–60 mM MgCl₂ with or without 0.15 mg/ml $C_{12}E_8$ or 15 μM A23187, as indicated. Subsequently Ca²⁺ was added to give 0.5 mM free concentration and incubated for various times, then diluted 10-fold with the above solution containing 5 mM EGTA without Ca²⁺. At 30 s after dilution, 4 μM TNP-AMP was added to determine the superfluorescence intensity. The representative time courses of loss of superfluorescence in $C_{12}E_8$ in 0.1 M K⁺ are shown in *inset*. The rate of Ca²⁺-induced $E2 \cdot BeF_3^-$ decomposition was determined by least-squares fit of a single exponential to the time course and plotted *versus* the Mg²⁺ concentration.

concentration retards the decomposition of $E1Ca_2 \cdot BeF_3^-$ to $E1Ca_2$ probably by inhibiting the Ca²⁺-replacement of Mg²⁺ at the unoccluded catalytic subsite[17].

Forward conversion of $E1Ca_2 \cdot BeF_3^-$ to $E2 \cdot BeF_3^-$ is favored in $C_{12}E_8$. Also in Fig. 6b, it can be seen that under conditions where $E1Ca_2 \cdot BeF_3^-$ is perfectly stable in A23187[17], the addition of $C_{12}E_8$ in place of A23187 produces the same proteolytic pattern as developed with $E2 \cdot BeF_3^-$ in $C_{12}E_8$ and Ca²⁺. The results reveal that the $E2 \cdot BeF_3^-$ state is produced and stabilized in $C_{12}E_8$ even under conditions that perfectly stabilize $E1Ca_2 \cdot BeF_3^-$ in the absence of $C_{12}E_8$. This was further verified by superfluorescence development and loss upon TNP-AMP addition in Fig. 6c, which was performed on the basis of previous findings[17] that $E1Ca_2 \cdot BeF_3^-$ rapidly decomposes to the non-fluorescent $E1Ca_2$ state upon TNP-AMP binding whereas $E2 \cdot BeF_3^-$ with bound TNP-AMP is stable, and also that the superfluorescence intensity is greater in $E2 \cdot BeF_3^-$ than in $E1Ca_2 \cdot BeF_3^-$ (by approximately 25%). In Fig. 6c, $E1Ca_2 \cdot BeF_3^-$ was first formed under the conditions in Fig. 6b without A23187 and $C_{12}E_8$, and then A23187 or $C_{12}E_8$ added. After 10 s, superfluorescence upon TNP-AMP addition was recorded. In A23187 or in its absence, superfluorescence development is followed by its rapid loss, which is due to $E1Ca_2 \cdot BeF_3^-$ decomposition to $E1Ca_2$ on TNP-AMP binding[17]. In $C_{12}E_8$, greater superfluorescence develops and its loss is considerably slower than in A23187. The results show again that in $C_{12}E_8$, $E2 \cdot BeF_3^-$ is formed even under conditions that perfectly stabilize $E1Ca_2 \cdot BeF_3^-$ (although $E2 \cdot BeF_3^-$ is slowly decomposed to the non-fluorescent $E1Ca_2$ state *via* $E1Ca_2 \cdot BeF_3^-$ in high Ca²⁺ and decomposition by TNP-AMP).

$E2P$ hydrolysis. In Fig. 7, the effects of $C_{12}E_8$, K⁺, and Mg²⁺ on the forward $E2P$ hydrolysis rate were examined at pH 7.4 and 6.0. Here $E2P$ was first formed in the reverse reaction of hydrolysis from the Ca²⁺-deprived $E2$ state and ³²P_i in 7 mM Mg²⁺ without or with $C_{12}E_8$ (or with A23187) in 20% (v/v) Me₂SO, conditions that favor $E2P$ formation. Then hydrolysis was initiated by a 20-fold dilution in non-radioactive P_i, various concentrations of Mg²⁺, and 0.1 M K⁺ (Fig. 7a) or Li⁺ (Fig. 7b) at the desired pH. In K⁺ at pH 7.4, $C_{12}E_8$ markedly retards hydrolysis as found previously at pH 7.5[27], and increasing Mg²⁺ concentration in $C_{12}E_8$ hardly affects the rate (perhaps a slight increase), but the cation decreases the rate in the absence of $C_{12}E_8$. Because this decrease is observed both without and with A23187 (an ionophore for Ca²⁺ and Mg²⁺) and because Me₂SO (used for the P_i-induced $E2P$ formation) does not permeabilize the SR membrane, the hydrolysis reaction rate itself is likely affected by Mg²⁺ at the cytoplasmic side. At pH 6.0 in K⁺, hydrolysis is much slower than at pH 7.4, as is well known[28], and $C_{12}E_8$ and Mg²⁺ have almost no effect on the slowed rate.

In the absence of K⁺ (Fig. 7b), $E2P$ hydrolysis at both pH 7.4 and 6.0 is much slower than in 0.1 M K⁺ (by ~10-fold at the respective pH), in agreement with the well-known acceleration of hydrolysis by specific K⁺ binding on the P domain[20,21]. In the absence of K⁺, hydrolysis in $C_{12}E_8$ is only slightly slower than that without $C_{12}E_8$. Mg²⁺ at ~10 mM somewhat increases the rate although the rate is still much slower than that in the presence of K⁺. In summary, induction of the detergent-stabilized state strongly inhibits hydrolysis at pH 7.4, but not following protonation of the transport sites at pH 6.0, and only in the presence of K⁺.

Discussion

Ca²⁺ transport by Ca²⁺-ATPase includes phosphorylated intermediates where Ca²⁺ is occluded at the transport sites and then released to the lumen, *i.e.* $E1P[Ca_2] \rightarrow E2P + Ca^{2+}$. During this process the A domain swings
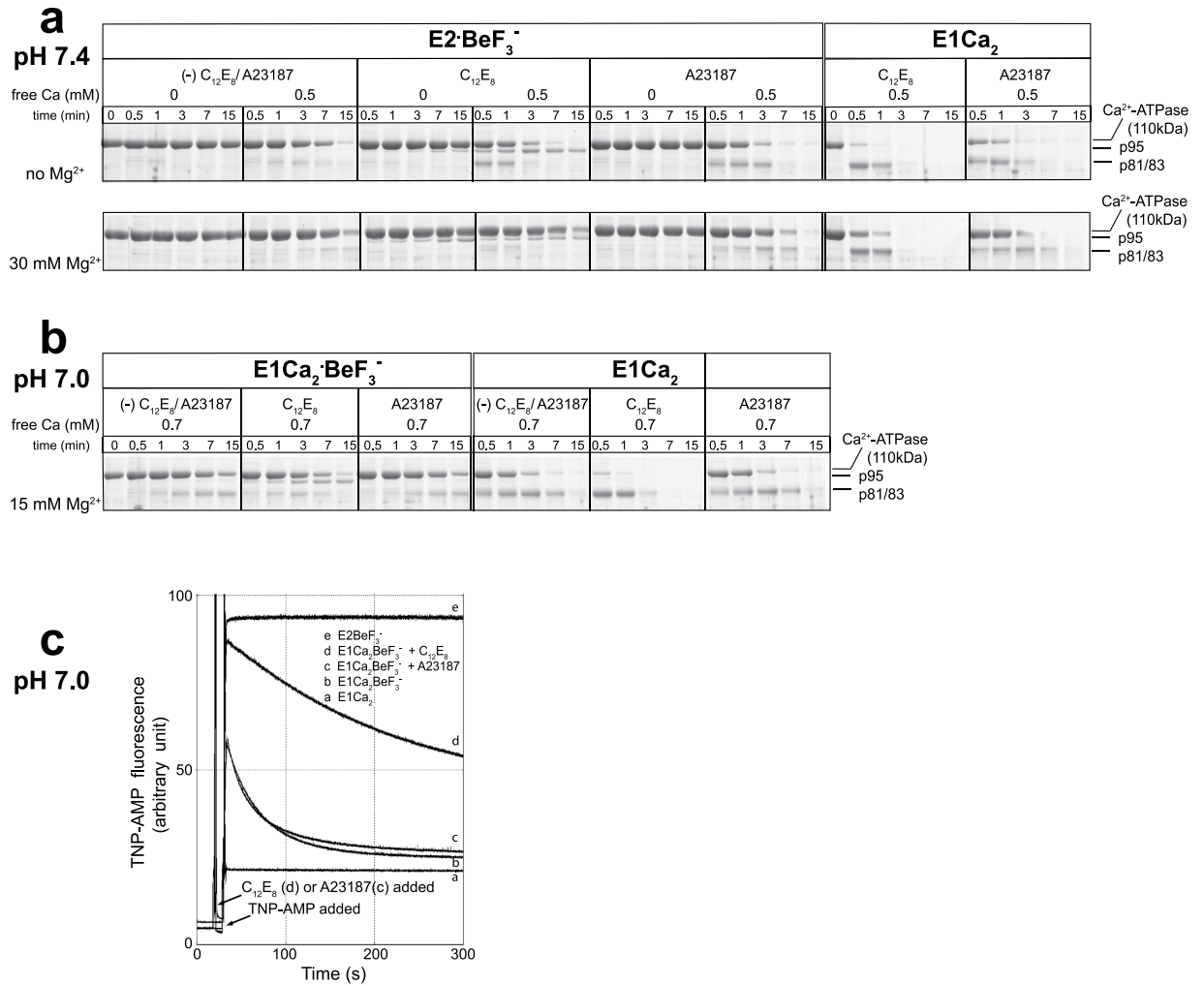
Figure 6. Luminal Ca^{2+}-effect on E2·BeF$_3^-$ in C$_{12}$E$_8$ (a) and formation and stabilization of E2·BeF$_3^-$ in forward conversion from E1Ca$_2$·BeF$_3^-$ in C$_{12}$E$_8$ (b,c). (**a**) E2·BeF$_3^-$ in SR vesicles was incubated without or with 0.15 mg/ml C$_{12}$E$_8$ or with 15 μM A23187 at 25 °C for 3 min in 30 mM MOPS/Tris (pH 7.4), 0.1 M LiCl, 0.5 mM EGTA, and 0 (upper panel) or 30 mM MgCl$_2$ (lower panel), then Ca^{2+} was added to give 0.5 mM free concentration. After 10 s, prtK was added at 0.5 mg/ml and incubated for indicated times. As a control, the BeF$_3^-$-free Ca^{2+}-ATPase in SR vesicles ("E1Ca$_2$") was subjected to the proteolysis in 0.5 mM free Ca^{2+}. (**b**) The prtK proteolysis was performed under the conditions that produce and perfectly stabilize E1Ca$_2$·BeF$_3^-$ [17], *i.e.* 30 mM MOPS/Tris (pH 7.0), 0.1 M KCl, 15 mM MgCl$_2$, and 0.7 mM CaCl$_2$ in the presence of 100 μM BeCl$_2$ and 2 mM KF without and with 15 μM A23187, and the effect of C$_{12}$E$_8$ was examined by including C$_{12}$E$_8$ without A23187, otherwise as in (**a**). The BeF$_3^-$-free Ca^{2+}-ATPase ("E1Ca$_2$") in A23187 and in C$_{12}$E$_8$ was subjected to proteolysis otherwise as above. Note that the slow decomposition of E2·BeF$_3^-$ in Ca^{2+} in the absence of A23187 and C$_{12}$E$_8$ (**a**) is probably due to slow Ca^{2+} permeation into the SR vesicles lumen [17]. (**c**) E1Ca$_2$·BeF$_3^-$ was produced by incubating SR vesicles for 30 min with 100 μM BeCl$_2$ and 2 mM KF in the absence of A23187 and C$_{12}$E$_8$ otherwise as in (**b**), then C$_{12}$E$_8$ or A23187 was added to give 0.02 mg/ml and 2.5 μM, respectively. At 10 s after this addition, TNP-AMP was added to give a saturating 4 μM, and the fluorescence monitored; trace b, without C$_{12}$E$_8$ and A23187; traces c and d, in A23178 and in C$_{12}$E$_8$, respectively. Trace e, the fluorescence monitored with E2·BeF$_3^-$ in the presence of 2 mM EGTA without adding Ca^{2+}. Trace a, the non-superfluorescent E1Ca$_2$ level (BeF$_3^-$-free Ca^{2+}-ATPase) in 4 μM TNP-AMP.

around and engages with the P domain and neck region of the protein at the cytoplasmic part of M2 (Fig. 1). The A-domain rotation inclines the P-domain by pulling an A/M1′-link, pushing M4 down towards the lumen to release the Ca^{2+} [8,18,19]. There is evidence that the gathering and interaction of A and P domains at the cytoplasmic part of M2 occurs progressively. Namely, changes, which are linked to deocclusion and opening of the luminal access channel with an affinity reduction, are followed by constrictions to limit access, protonation, and finally closure, and all these changes are synchronized with catalytic site preparations for hydrolysis [4,13,15,17–19]. Part of the development is seen with the Leu[119] prtK cleavage site, being exposed in E2PCa$_2$, hidden in E2P, E2~P‡ and E2·P$_i$, and exposed again in E2 [4,18,19]. We found here that non-solubilizing concentrations of C$_{12}$E$_8$ uncovers the Leu[119] prtK site of E2P, as depicted in its analog E2·BeF$_3^-$. This indicates that membrane perturbation drives the
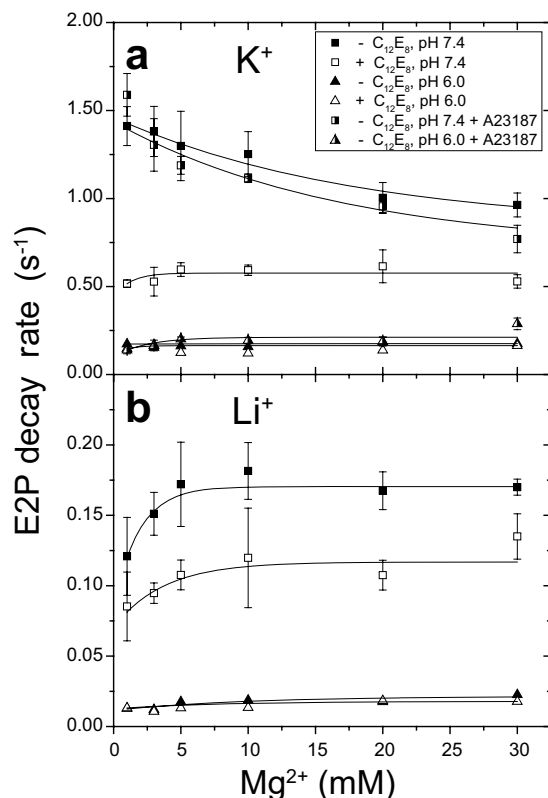
Figure 7. Effects of $C_{12}E_8$ and various factors on E2P hydrolysis. SR vesicles were phosphorylated with 0.1 mM $^{32}P_i$ at 25 °C for 10 min in 5 μl of a mixture containing 0.3 mg protein/ml with or without 3 μM A23187 as indicated, 1 mM EGTA, 7 mM MgCl$_2$, 30 mM MOPS/Tris (pH 7.4) or MES/Tris (pH 6.0), and 20% (v/v) Me$_2$SO. The mixture was then cooled, and a small volume of $C_{12}E_8$ was added to give 0.1 mg/ml (1/3 (w/w) of the protein) to the indicated samples. Subsequently, the samples were diluted at 0 °C by the addition of 95 μl of a mixture containing 0.1 mM non-radioactive P_i, 105 mM KCl (**a**) or LiCl (**b**), 1 mM EGTA, 1–30 mM MgCl$_2$, and 50 mM MOPS/Tris (pH 7.4) or MES/Tris (pH 6.0), as indicated with different symbols. The E2P hydrolysis rate was determined as described under "METHODS" and plotted *versus* Mg^{2+}concentration. Note the difference in the scale of the ordinate in (**a**) and (**b**).

intermediate towards one more like that with bound Ca^{2+}, and points to an earlier catalytic intermediate with a looser arrangement in the head region, as expected for early engagement of the rotated A domain. The responsiveness of E2P to membrane perturbation and the detergent-induced state to ligand binding (Ca^{2+}, Mg^{2+}, K$^+$, H$^+$, and TG) through changes in exposure of the Leu[119] prtK site at the cytoplasmic part of M2 points to flexible and rather unstable forms. These properties are due most probably not only to its unoccupied transport sites and associated circle of negative charges, but also to a loose meeting of domains and neck region with largely unsecured interactions at the cytoplasmic part of M2. The downward thrust of M4 (by a full turn of an α-helix[8]), together with M3, is probably partly stabilized by surrounding phospholipids and insertion of non-ionic detergent between them could be disruptive. In the head region the interactions at Leu[119] involve the formation of Y122-HC, a hydrophobic interaction network of Tyr[122]/Leu[119] with the A and P domains and A/M3-linker involving seven residues (Fig. 2). As mentioned above, the interactions are likely progressive, loose at first as the A domain engages followed by incremental tightening in E2P to the fully stabilized state in E2~P‡ and E2·P$_i$. Indeed, in the E2·BeF$_3^-$ crystal structures (formed in the presence of $C_{12}E_8$) with the bound Mg^{2+} or with protonation without the Mg^{2+}, Leu[119]/Tyr[122] on M2 are close but not yet associated with the five other gathered residues involved in Y122-HC formation. The knitting of Leu[119] and Tyr[122] with the other residues is seen in the crystal structures of analogs of the next intermediates, E2~P‡ and E2·P$_i$. Accumulating interactions fit perfectly with the staggered changes at the luminal transport sites, from closed to open to closed again.

Stabilization of the early detergent-induced state is seen in the forward direction of catalysis coming from E1PCa$_2$ (E1Ca$_2$·BeF$_3^-$) and in the backward direction with Ca^{2+} binding to the luminal sites of E2P (E2·BeF$_3^-$), using both TNP-AMP superfluorescence and the prtK sites as probes. Our results suggest that the E2·BeF$_3^-$ structural state favored in $C_{12}E_8$ and stabilized by Mg^{2+} represents one between E1PCa$_2$ and Ca^{2+}-released E2P, *i.e.* the transient E2P state immediately following Ca^{2+} release denoted as E2P* with luminally open and vacant low affinity transport sites (E2P*Ca$_2 \rightarrow E$2P* in Fig. 8). $C_{12}E_8$ stabilizes the E2P* state and thereby retards both the luminal Ca^{2+}-induced reverse conversion and the forward hydrolysis of E2P at pH 7.4. Mg^{2+} binding probably prevents luminal Ca^{2+}-access and consequent reverse conversion (Figs 3,5 and 6). This Mg^{2+} is likely at or near the luminally open Ca^{2+} transport sites (in addition to Mg^{2+} occluded at the catalytic subsite in E2·BeF$_3^-$ and E2P) as actually seen in the E2·BeF$_3^-$ crystal produced in a high concentration of Mg^{2+} [11]. The Mg^{2+} probably
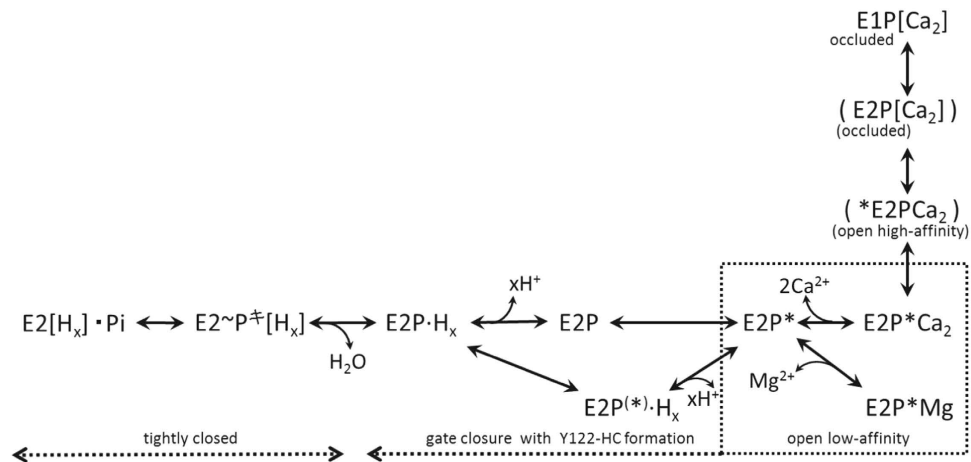
Figure 8. EP processing and gating. The effects of $C_{12}E_8$, luminal Ca^{2+}, and Mg^{2+} found in this study are summarized. $E2P[Ca_2]$ ($E2P$ with occluded Ca^{2+}) and $^*E2PCa_2$ ($E2P$ with luminally open gate and with bound Ca^{2+} yet at a high affinity) were previously identified by the elongation of the A/M1′-linker[18,19] and by substitutional mutation of Leu^{119} and Tyr^{122} [15], but they are transient intermediates and have never been trapped or identified in wild type[15,18,19]; therefore they are shown in brackets. The $E2P$ structural states found in this study at pH 7.4, the Leu^{119}-cleavable state and the prtK-resistant state are denoted as $E2P^*$ and $E2P$, respectively. The prtK-resistant state found in $C_{12}E_8$ at pH 6.0 (*i.e.* with protonation of the transport sites) is denoted as $E2P(^*)$. Note that Y122-HC formation on gathering of Leu^{119}/Tyr^{122} on M2 with engaged A and P domains occurs progressively during $E2P$ processing and couples with luminal gating (see more in "Discussion").

manifests itself in the competitive inhibition by Mg^{2+} of luminal Ca^{2+}-induced reverse isomerization $E2P + 2Ca^{2+} \rightarrow E1PCa_2$[29]. Notably also, the dephosphorylated $E1$ state is able to accommodate one Mg^{2+} at the transport sites and forms $E1 \cdot Mg$, which favors high affinity Ca^{2+}-binding resulting in a rapid $E2 \rightarrow E1 \cdot Mg \rightarrow E1Ca_2$ transition[30,31] (Fig. 1). Thus it seems that Mg^{2+} binds at the empty transport sites both in the unphosphorylated and phosphorylated states and modifies transport function.

The $E2 \cdot BeF_3^-$ structures revealed in $C_{12}E_8$ and in A23187 at pH 7.4 reflect $E2P^*$ and $E2P$ respectively in Fig. 8 on the basis of prtK-resistance. Analysis of the Mg^{2+} inhibition of luminal Ca^{2+}-induced reverse conversion of $E2 \cdot BeF_3^-$ in Figs 5 and 6 indicates that Mg^{2+} accesses $E2P^*$ with a much higher affinity than $E2P$. Thus the transport sites appear more open and accessible to Mg^{2+} on the luminal side in the Leu^{119}-site cleavable $E2P^*$ state than in the prtK-resistant $E2P$ ground state. In fact, in the $E2 \cdot BeF_3^-$ crystal with bound Mg^{2+} at the transport sites, the sites are actually more open to the lumen than in the structure without Mg^{2+} (Fig. 2). Note also that in $E2 \cdot AlF_4^-$ and $E2 \cdot MgF_4^{2-}$ ($E2 \sim P^\ddagger$ and $E2 \cdot P_i$) and in $E2 \cdot BeF_3^-$ with bound TG, Ca^{2+} cannot bind as the luminal gate is tightly closed[4,7,8], and the Leu^{119}-site is completely resistant to prtK regardless of the presence of $C_{12}E_8$ (Fig. 3). These findings suggest that the structural change reflected by prtK resistance at Leu^{119} is associated with luminal gating, supporting the above conclusion that substantial luminal gate closure occurs in $E2P^* \rightarrow E2P$, which probably involves gathering of Leu^{119}/Tyr^{122} with the engaged A and P domains to accomplish the Y122-HC network. Then the passage is completely sealed in $E2 \sim P^\ddagger$ and $E2 \cdot P_i$ ($E2 \cdot AlF_4^-$ and $E2 \cdot MgF_4^{2-}$)[4].

Previous kinetic analysis of the luminal Ca^{2+}-induced reverse isomerization $E2P + 2Ca^{2+} \rightarrow E1PCa_2$ indicated[14] that the luminal Ca^{2+} access to the transport sites in $E2P$ is rate-limiting. This is described in Fig. 8 with the equilibrium $E2P^* \leftrightarrow E2P$, where the former state is more open and the latter relatively closed. This view agrees with our finding on the Ca^{2+} release kinetics $E1PCa_2 \rightarrow E2PCa_2 \rightarrow E2P + 2Ca^{2+}$ [15] that the $E2P$ structure proceeds from a luminally open state for Ca^{2+} release (corresponding to $E2P^*$ in Fig. 8) to a closed state ($E2P$) with the structural contribution of Leu^{119}/Tyr^{122}. The observation that Mg^{2+} hardly alters the forward $E2P$ hydrolysis rate in $C_{12}E_8$ (Fig. 7a) can be accounted for by a rapid Mg^{2+} binding/release relative to the hydrolysis reaction process, and implies that Mg^{2+} binding favors the forward reaction.

At pH 6.0 in which the transport sites are protonated, the Leu^{119}-site is completely resistant to prtK regardless of the presence of $C_{12}E_8$, and the $E2P$ hydrolysis rate is not affected by $C_{12}E_8$. In Fig. 8, the protonated structural state with the prtK-resistance revealed in $C_{12}E_8$ is denoted as $E2P(^*)$ to be discriminated from the prtK-cleavable $E2P^*$ state without protonation. Protonation neutralizes charges at the Ca^{2+}-binding sites and stabilizes the arrangement of transmembrane helices *via* a hydrogen bonding network[8], which lowers Ca^{2+}-accessibility (without completely closing the gate as seen in the $E2 \cdot BeF_3^-$ crystal formed at pH 5.7[8]). The protonated state proceeds promptly to subsequent hydrolysis with tight gate closure $E2P + H_2O \rightarrow E2 \sim P^\ddagger$ ($E2 \cdot BeF_3^- \rightarrow E2 \cdot AlF_4^-$), as indicated previously by kinetic analysis of $E2P$ hydrolysis[5].

K^+ in the presence of $C_{12}E_8$ accelerates both forward $E2P$ hydrolysis and luminal Ca^{2+}-induced reverse conversion of $E2 \cdot BeF_3^-$ (Figs 5 and 7). These findings are in complete agreement with the known role of specific K^+ binding on the P domain in accelerating both forward hydrolysis[20,21] and luminal Ca^{2+}-induced reverse conversion of $E2P$[14]. K^+ binding likely destabilizes both $E2P$ and $E2P^*$ in Fig. 8, thus promoting rapid transport.

Finally, induction of the detergent-stabilized state, an early intermediate to ground state E2P, shows how phospholipids are intimately involved in the latter's stabilization. Membrane perturbation effects during the transport cycle may be under-appreciated as fundamental to the mechanism.

Methods

Preparation of SR vesicles and treatment with BeF$_x$, AlF$_x$, and MgF$_x$. SR vesicles were prepared from rabbit skeletal muscle as described[32,33], in which all the methods were carried out in accordance with institutional laws and regulations of the Asahikawa Medical University and the experimental protocols were approved by the Animal Experimentation Ethics Committee of the Asahikawa Medical University (license number 16006). The content of the phosphorylation site in the vesicles and the Ca^{2+}-dependent ATPase activity were determined as described[32,33]. $E2 \cdot BeF_3^-$, $E2 \cdot AlF_4^-$, and $E2 \cdot MgF_4^{2-}$ were produced by incubating the SR vesicles with the respective metal fluoride and by washing the unbound ligands as described previously[4].

Formation and hydrolysis of E2P. The SR vesicles were phosphorylated with 0.1 mM ^{32}P$_i$ at 25 °C for 10 min in 20% (v/v) Me$_2$SO in the absence of Ca^{2+}, after which the samples were cooled and diluted 20-fold by a solution containing 2.1 mM non-radioactive P$_i$ to initiate the hydrolysis of ^{32}P$_i$-labeled E2P, otherwise as described in detail in the legend to Fig. 7. The reaction was quenched with ice-cold trichloroacetic acid containing P$_i$. The precipitated proteins were separated by 5% SDS-PAGE at pH 6.0 according to Weber and Osborn[34]. The radioactivity associated with the separated Ca^{2+}-ATPase was quantified by digital autoradiography as described[35]. Rapid kinetics measurement of hydrolysis was performed with a handmade rapid mixing apparatus and the rate of hydrolysis was determined with the least-squares fit to a single exponential, as described[35].

Proteolytic analysis. SR vesicles (0.45 mg/ml protein) were subjected to proteolysis at 25 °C by addition of trypsin (at 0.3 mg/ml, L-1-tosylamido-2-phenylethyl chloromethyl ketone-treated) or proteinase K (prtK, at 0.1 mg/ml, Sigma) as described previously[6,16], otherwise as indicated in the figure legends. The proteolysis was terminated by trichloroacetic acid, and the samples were subjected to Laemmli SDS-polyacrylamide gel electrophoresis[36], and densitometric analyses of the gels stained with Coomassie Brilliant Blue R-250, as described[6,16]. The degradation rate of 110-kDa ATPase chain with prtK was determined by least-squares fit of a single exponential to the time course (0–150 min) as described previously[16].

Fluorescence measurements. The TNP-AMP fluorescence of the Ca^{2+}-ATPase (0.06 mg/ml protein, TNP-AMP from Molecular Probes® Life Technologies) was measured on a RF-5300PC spectrofluorophotometer (Shimadzu, Kyoto, Japan) with excitation and emission wavelengths 408 and 540 nm (with band widths 5 and 10 nm), as described previously[4].

Miscellaneous. Protein concentrations were determined by the method of Lowry et al.[37] with bovine serum albumin as a standard. Three-dimensional models of the enzyme were reproduced by the program VMD[38]. The values presented are the mean ± s.d. (n = 3–4).

References

1. Toyoshima, C. Structural aspects of ion pumping by Ca^{2+}-ATPase of sarcoplasmic reticulum. *Arch. Biochem. Biophys.* **476,** 3–11 (2008).
2. Toyoshima, C. How Ca^{2+}-ATPase pumps ions across the sarcoplasmic reticulum membrane. *Biochim. Biophys. Acta* **1793,** 941–946 (2009).
3. Møller, J. V., Olesen, C., Winther, A.-M. L. & Nissen, P. The sarcoplasmic Ca^{2+}-ATPase: design of a perfect chemi-osmotic pump. *Q. Rev. Biophys.* **43,** 501–566 (2010).
4. Danko, S., Yamasaki, K., Daiho, T. & Suzuki, H. Distinct natures of beryllium fluoride-bound, aluminum fluoride-bound, and magnesium fluoride-bound stable analogues of an ADP-insensitive phosphoenzyme intermediate of sarcoplasmic reticulum Ca^{2+}-ATPase. *J. Biol. Chem.* **279,** 14991–14998 (2004).
5. Seekoe, T., Peall, S. & McIntosh, D. B. Thapsigargin and dimethyl sulfoxide activate medium Pi - HOH oxygen exchange catalyzed by sarcoplasmic reticulum Ca^{2+}-ATPase. *J. Biol. Chem.* **276,** 46737–46744 (2001).
6. Danko, S., Yamasaki, K., Daiho, T., Suzuki, H. & Toyoshima, C. Organization of cytoplasmic domains of sarcoplasmic reticulum Ca^{2+}-ATPase in E$_1$P and E$_1$ATP states: a limited proteolysis study. *FEBS Lett.* **505,** 129–135 (2001).
7. Toyoshima, C., Nomura, H. & Tsuda, T. Lumenal gating mechanism revealed in calcium pump crystal structures with phosphate analogues. *Nature* **432,** 361–368 (2004).
8. Toyoshima, C., Norimatsu, Y., Iwasawa, S., Tsuda, T. & Ogawa, H. How processing of aspartylphosphate is coupled to lumenal gating of the ion pathway in the calcium pump. *Proc. Natl. Acad. Sci. USA* **104,** 19831–19836 (2007).
9. Daiho, T., Yamasaki, K., Danko, S. & Suzuki, H. Second transmembrane helix (M2) and long range coupling in Ca^{2+}-ATPase. *J. Biol. Chem.* **289,** 31241–31252 (2014).
10. Olesen, C., Sørensen, T. L., Nielsen, R. C., Møller, J. V. & Nissen, P. Dephosphorylation of the calcium pump coupled to counterion occlusion. *Science* **306,** 2251–2255 (2004).
11. Olesen, C. et al. The structural basis of calcium transport by the calcium pump. *Nature* **450,** 1036–1042 (2007).
12. Yamasaki, K., Daiho, T., Danko, S. & Suzuki, H. Multiple and distinct effects of mutations of Tyr^{122}, Glu^{123}, Arg^{324}, and Arg^{334} involved in interactions between the top part of second and fourth transmembrane helices in sarcoplasmic reticulum Ca^{2+}-ATPase. *J. Biol. Chem.* **279,** 2202–2210 (2004).
13. Wang, G., Yamasaki, K., Daiho, T. & Suzuki, H. Critical hydrophobic interactions between phosphorylation and actuator domains of Ca^{2+}-ATPase for hydrolysis of phosphorylated intermediate. *J. Biol. Chem.* **280,** 26508–26516 (2005).
14. Yamasaki, K., Wang, G., Daiho, T., Danko, S. & Suzuki, H. Roles of Tyr^{122}-hydrophobic cluster and K$^+$ binding in Ca^{2+}-releasing process of ADP-insensitive phosphoenzyme of sarcoplasmic reticulum Ca^{2+}-ATPase. *J. Biol. Chem.* **283,** 29144–29155 (2008).
15. Yamasaki, K., Daiho, T., Danko, S. & Suzuki, H. Assembly of a Tyr^{122} hydrophobic cluster in sarcoplasmic reticulum Ca^{2+}-ATPase synchronizes Ca^{2+} affinity reduction and release with phosphoenzyme isomerization. *J. Biol. Chem.* **290,** 27858–27879 (2015).
16. Danko et al. ADP-insensitive phosphoenzyme intermediate of sarcoplasmic reticulum Ca^{2+}-ATPase has a compact conformation resistant to proteinase K, V8 protease and trypsin. *FEBS Lett.* **489,** 277–282 (2001).

17. Danko, S., Daiho, T., Yamasaki, K., Liu, X. & Suzuki, H. Formation of the stable structural analog of ADP-sensitive phosphoenzyme of Ca^{2+}-ATPase with occluded Ca^{2+} by beryllium fluoride. *J. Biol. Chem.* **284,** 22722–22735 (2009).
18. Daiho, T., Yamasaki, K., Danko, S. & Suzuki, H. Critical role of $Glu^{40}-Ser^{48}$ loop linking actuator domain and first transmembrane helix of Ca^{2+}-ATPase in Ca^{2+} deocclusion and release from ADP-insensitive phosphoenzyme. *J. Biol. Chem.* **282,** 34429–34447 (2007).
19. Daiho, T., Danko, S., Yamasaki, K. & Suzuki, H. Stable structural analog of Ca^{2+}-ATPase ADP-insensitive phosphoenzyme with occluded Ca^{2+} formed by elongation of A-domain/M1'-linker and beryllium fluoride binding. *J. Biol. Chem.* **285,** 24538–24547 (2010).
20. Shigekawa, M. & Pearl, L. J. Activation of calcium transport in skeletal muscle sarcoplasmic reticulum by monovalent cations. *J. Biol. Chem.* **251,** 6947–6952 (1976).
21. Sorensen, T. L. *et al.* Localization of a K^+-binding site involved in dephosphorylation of the sarcoplasmic reticulum Ca^{2+}-ATPase. *J. Biol. Chem.* **279,** 46355–46358 (2004).
22. Inesi, G., Lewis, D., Toyoshima, C., Hirata, A. & de Meis, L. Conformational fluctuations of the Ca^{2+}-ATPase in the native membrane environment. Effects of pH, temperature, catalytic substrates, and thapsigargin. *J. Biol. Chem.* **283,** 1189–1196 (2008).
23. Toyoshima, C. & Nomura, H. Structural changes in the calcium pump accompanying the dissociation of calcium. *Nature* **418,** 605–611 (2002).
24. Kato, S. *et al.* Val^{200} residue in $Lys^{189}–Lys^{205}$ outermost loop on the A domain of sarcoplasmic reticulum Ca^{2+}-ATPase is critical for rapid processing of phosphoenzyme intermediate after loss of ADP sensitivity. *J. Biol. Chem.* **278,** 9624–9629 (2003).
25. Dupont, Y. & Pougeois, R. Evaluation of H_2O activity in the free or phosphorylated catalytic site of Ca^{2+}-ATPase. *FEBS Lett.* **156,** 93–98 (1983).
26. Toyoshima, C., Yonekura, S., Tsueda, J. & Iwasawa, S. Trinitrophenyl derivatives bind differently from parent adenine nucleotides to Ca^{2+}-ATPase in the absence of Ca^{2+}. *Proc. Natl. Acad. Sci. USA.* **108,** 1833–1838 (2011).
27. Champeil, P. *et al.* Kinetic characterization of the normal and detergent-perturbed reaction cycles of the sarcoplasmic reticulum calcium pump. Rate-limiting step(s) under different conditions. *J. Biol. Chem.* **261,** 16372–16384 (1986).
28. Wakabayashi, S., Ogurusu, T. & Shigekawa, M. Modulation of the hydrolysis rate of the ADP-insensitive phosphoenzyme of the sarcoplasmic reticulum ATPase by H^+ and Mg^{2+}. *J. Biol. Chem.* **262,** 9121–9129 (1987).
29. Bishop, J. E. & Al-Shawi, M. K. Inhibition of sarcoplasmic reticulum Ca^{2+}-ATPase by Mg^{2+} at high pH. *J. Biol. Chem.* **263,** 1886–1892 (1988).
30. Toyoshima, C. *et al.* Crystal structures of the calcium pump and sarcolipin in the Mg^{2+}-bound E1 state. *Nature* **495,** 260–264 (2013).
31. Winther, A. M. *et al.* The sarcolipin-bound calcium pump stabilizes calcium sites exposed to the cytoplasm. *Nature* **495,** 265–269 (2013).
32. Nakamura, S., Suzuki, H. & Kanazawa, T. The ATP-induced change of tryptophan fluorescence reflects a conformational change upon formation of ADP-sensitive phosphoenzyme in the sarcoplasmic reticulum Ca^{2+}-ATPase. Stopped-flow spectrofluorometry and continuous flow-rapid quenching method. *J. Biol. Chem.* **269,** 16015–16019 (1994).
33. Barrabin, H., Scofano, H. M. & Inesi, G. Adenosinetriphosphatase site stoichiometry in sarcoplasmic reticulum vesicles and purified enzyme. *Biochemistry* **23,** 1542–1548 (1984).
34. Weber, K. & Osborn, M. The reliability of molecular weight determinations by dodecyl sulfate-polyacrylamide gel electrophoresis. *J. Biol. Chem.* **244,** 4406–4412 (1969).
35. Daiho, T., Suzuki, H., Yamasaki, K., Saino, T. & Kanazawa, T. Mutations of Arg^{198} in sarcoplasmic reticulum Ca^{2+}-ATPase cause inhibition of hydrolysis of the phosphoenzyme intermediate formed from inorganic phosphate. *FEBS Lett.* **444,** 54–58 (1999).
36. Laemmli, U. K. Cleavage of structural proteins during the assembly of the head of bacteriophage T4. *Nature* **227,** 680–685 (1970).
37. Lowry, O. H., Rosebrough, N. J., Farr, A. L. & Randall, R. J. Protein measurement with the folin phenol reagent. *J. Biol. Chem.* **193,** 265–275 (1951).
38. Humphrey, W., Dalke, A. & Schulten, K. VMD: visual molecular dynamics. *J. Mol. Graph.* **14,** 33–38 (1996).
39. Juul, B. *et al.* Do transmembrane segments in proteolyzed sarcoplasmic reticulum Ca^{2+}-ATPase retain their functional Ca^{2+} binding properties after removal of cytoplasmic fragments by proteinase K? *J. Biol. Chem.* **270,** 20123–20134 (1995).
40. Brandl, C. J., Green, N. M., Korczak, B. & MacLennan, D. H. Two Ca^{2+} ATPase genes: homologies and mechanistic implications of deduced amino acid sequences. *Cell* **44,** 597–607 (1986).

Acknowledgements

Author Contributions

S.D. and H.S. conceived and coordinated the study and wrote the paper. S.D., K.Y. and H.S. designed, performed and analyzed the experiments. T.D. provided critical discussion. All authors reviewed the results and approved the final version of the manuscript.

Additional Information

Competing financial interests: The authors declare no competing financial interests.

How to cite this article: Danko, S. *et al.* Membrane Perturbation of ADP-insensitive Phosphoenzyme of Ca^{2+}-ATPase Modifies Gathering of Transmembrane Helix M2 with Cytoplasmic Domains and Luminal Gating. *Sci. Rep.* **7,** 41172; doi: 10.1038/srep41172 (2017).

Publisher's note: Springer Nature remains neutral with regard to jurisdictional claims in published maps and institutional affiliations.